IMPROVING NO$_2$ SENSITIVITY OF POROUS SILICON BY FUNCTIONALIZATION ITS SURFACE WITH COPPER AS CATALYST

Iftikhar M. Ali[1, *], Massar A. Kaood[1, **]
[1]Dept. of phys., College of science, Baghdad University., IRAQ
[*]iftikhariq@gmail.com, [**]masar91abidz@gmail.com

ABSTRACT: *In this work, porous silicon gas sensor hs been fabricated on n-type crystalline silicon (c-Si) wafers of (100) orientation denoted by n-PS using electrochemical etching (ECE) process at etching time 10 min and etching current density 40 mA/cm^2. Deposition of the catalyst (Cu) is done by immersing porous silicon (PS) layer in solution consists of 3ml from (Cu) chloride with 4ml (HF) and 12ml (ethanol) and 1 ml (H$_2$O$_2$). The structural, morphological and gas sensing behavior of porous silicon has been studied. The formation of nanostructured silicon is confirmed by using X-ray diffraction (XRD) measurement as well as it shows the formation of an oxide silicon layer due to chemical reaction. Atomic force microscope for PS illustrates that the pores have sphere-like shape and the porous layers have sponge-like appearance. Sensing behavior is studied for PS before and after fictionalization with copper at different operating temperatures and it is found that the maximum sensitivity is (64516.82%) after fictionalization with Cu at T=250 ºC.*

Keywords: Porous silicon, Porosity, Gas sensor, Sensitivity, and NO$_2$ toxic gas.

I.   INTRODUCTION

Among scientists and technologists, porous silicon (PS) material has become a popular material, and has been applied in various fields during the past two decades, such as emitting materials in optoelectronics, bone growth media in biology, gas and humidity sensors in chemistry, surface texturization in photovoltaic's or sacrificial layers in micromachining [1]. In the early 1990s, the discovery of room temperature photoluminescence from porous silicon by Canham started a renewed interest in this material [2]. Since then, porous silicon has been developed as a means of increasing the functionality of silicon technology. New types of porous silicon have been added into the family and its applications now span the fields of electronics, optics, optoelectronics, micromachining and biomedical engineering, nanoporous materials are classified in three main groups depending on their pore dimension (a) Microporous materials (d<2 n), (b) Mesoporous materials (2<d<50 nm) and (c) Macroporous systems (d>50 nm) [3]. The physical properties of porous silicon are fundamentally determined by the shape, diameter of pores, porosity, and the thickness of the formed porous layer. Porous silicon (PS) has attracted attention for gas sensing due to the unique combination of advantageous properties. There is an increasing demand for sensitive and selective gas sensing with applications in toxic gas detection and manufacturing process monitoring. The NOx is a toxic gas associated with air pollution, combustion and respiratory disease. Exhaled nitric oxide is correlated with asthmatic conditions such as airway inflammation and with the potential to provide rapidly accessed noninvasive disease detection [4].

In this work, introducing transition metal (TM), such as copper (Cu), into the PS structure modifies the surface state and creates a sub-energy band level, which improves sensing properties for NO$_2$ gas. Thus, an appropriate amount of Cu can optimize the electrical and sensing properties of pure PS.

II.   MATERIAL AND METHODS

PS layer was prepared by electrochemical anodic etching of arsenic doped (n-type) (100) oriented silicon substrate with a resistivity 0.001-0.005 Ω.cm. Before electrochemical etching process, the silicon wafers are cleaned with a solution HF:

ethanol with a volume ratio 1:10 for a period of about 1 minute. Thin layer of Ag has been deposited on the wafers by electrodeposition method where wafers are immersed into a solution of 0.1 M silver nitrate solution that dissolved in 100 ml of distilled water. Silicon connected to the circuit with power supply in which the faces of silicon opposite to platinum pole that connected to the positive end of the power supply with 3V that supplies current equals to 20 mA for 5 minutes. Silicon connected to the negative end of power supply, this Ag atoms work as a catalyst making the etching process easier**.** Then silicon wafer is cut into small pieces (1.3 × 1.3 cm^2). The electrochemical etching process has been carried out at room temperature using Teflon materials which are adopted to form the main-body of hydrofluoric acid (HF) based electrolyte container. A mixture containing HF (40%), ethanol of (99%) and hydrogen peroxide (HF: ethanol: H$_2$O$_2$ = 1:4:1 volume ratio) were used as the etching solvent for all PS samples. H$_2$O$_2$ was added to the (HF) solution in order to improve the wet ability of the acid and to allow diffusion for the F ions into pores and to improve the PS layer uniformity by removing the hydrogen bubbles and helps to moisten silicon surface and improve reproducibility [5]. Porous process is done under tungsten light of 100 Watt for n-type Si to supply holes for etching reaction where the existence of light generates holes to the electrolyte solution and the ideal formation the pore. The anodization is done at room temperature under constant time of 10 minutes for etching current density 40 mA/cm^2.
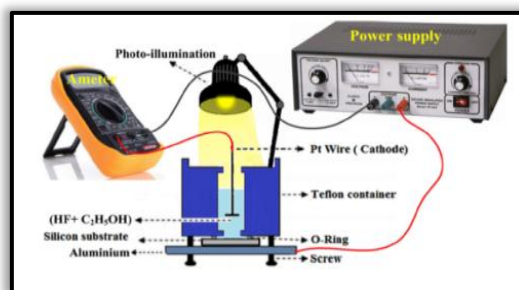
Figure 1-The electrochemical etching set-up

For The process of fictionalization PS by (Cu) within the pores is done as following:

1. In this method, 0.1 M from cerium chloride have been prepared separately in distilled water, then quantities consists of 3ml of (Cu) chloride solutions, 4ml (HF), 12 ml (ethanol), 1ml (H_2O_2) are mixed which is denoted by (**solution A**).

2. After preparation PS samples, the freshly PS substrates are then dipped in 10% HF solution for 10 sec and immediately are dipped into chloride solution of cerium (i.e. **solution A**) to passivity the surface states. Subsequently the samples were rinsed gently by DI water and dried followed by annealing in air at 110^oC inside an electric oven for 1 hour to evaporate the residual solvent present in the sample. This procedure is illustrated in figure (2).
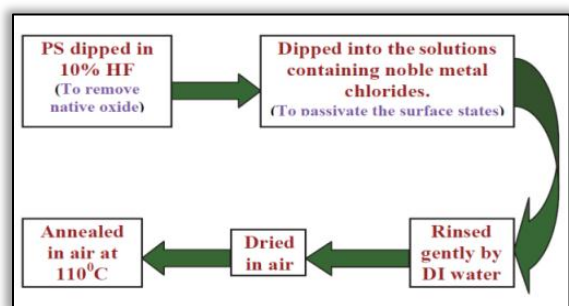
Figure (2): Flow chart for porous silicon surface modification with metal

III. RESULT AND DISCUSSION
3.1. X-Ray Diffraction Results

Figure (3) shows the comparison between XRD pattern for Si before and after etching process one can observe that Si has high and sharp peak intensity and this peak will have broadening with low intensity due to nanosize

structure and strain effect after porous process for silicon n-type of (100) direction at current density 40 mA/cm^2 and constant etching time of 10 min. XRD pattern (at the right of figure 3) shows the formation of porous silicon where the strong peak of Si is observed at 2θ = 68.002º to n-type Si for (100) direction and shows that there is non-uniform strain happened in the lattice[6] also there are two phases in the lattice ; Si and SiO_2. The crystallite size is calculated by using Debye Scherrer formula in equation (1):

D=K λ /β cos θ..... (1)

where λ is the X-ray wavelength (1.54Å), β is full width at half maximum (FWHM), θ is Bragg's angle, K is the Scherrer 's constant ≈ was ranged from (0.9 to 1) depends on geometry of structure.

From Table (1) it can be noticed there is a decrease in crystallite size this is may be the exits of light that generates holes to the electrolyte solution and the ideal formation the pore, also the decrease in the average of the crystallite size indicate that there is an increase in the porosity [7]. Also the decrease in nano sizes pore may be because the pore propagation into the crystal volume is a process that is controlled not only by the electrochemical factors, but also by mechanical stresses, strain and hydrogen-related defects in Si

lattice [8]. XRD results show the existing of SiO_2 phase inside Si lattice as illustrated in Table (1) which is evidence to porous formation.
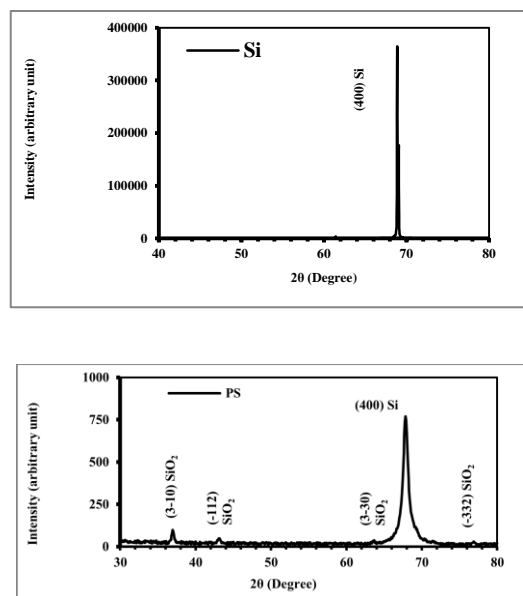
Figure (3): X-ray diffraction for Si (upper) and for n-PS (down)

3.2. Atomic Force Microscopy (AFM) Analysis Results

The morphological properties of n- PS samples prepared with the current density 40 mA/cm^2 at 10 min etching time are shown in figures (4). Pores are observed on the surface of the layer to be distributed uniformly. The pores have sphere-like shape and the porous layers have sponge-like appearance. The average pore diameter appears in good agreement with what expected for a meso-porous layer and we found that when increasing current density of etching the porosity of PS increases as present in table (2).

In general, the pore size distribution has Gaussian shape that shown uniform size along the etched surface for n-PS.

3.3. Element Mapping by EDS Technique

An element map is an image showing the spatial distribution of elements in a sample. Because it is acquired from a polished section, it is a 2D section through the unknown sample. Element maps are extremely useful for displaying element distributions in textural context, particularly for showing compositional zonation. An EDX analysis of the whole spatial region was performed to find out the elements distribution in the measured area. Note that the elements within the etching are uniformly distributed as shown in Figure (5).

Table (1): Structural parameters: 2θ, dhkl, (hkl), FWHM and D of n-PS at current density40 mA/cm² and 10 min etching time.

J (mA/cm²)	2θ (Deg)	FWHM (Deg.)	dhkl Exp.(Å)	D (nm)	hkl	dhkl Std.(Å)	Phase	Card No.
40	36.9786	0.3231	2.4290	25.9	(3-10)	2.4248	Tric. SiO₂	96-720-2757
	43.1028	0.3714	2.0970	23.0	(-112)	2.0749	Tric. SiO₂	96-720-2757
	64.1246	0.3953	1.4511	23.7	(3-30)	1.4548	Tric. SiO₂	96-720-2757
	67.8465	1.2533	1.3803	7.6	(400)	1.3577	Cub. Si	96-410-4918
	77.4634	0.2554	1.2312	39.9	(-332)	1.2382	Tric. SiO₂	96-720-2757
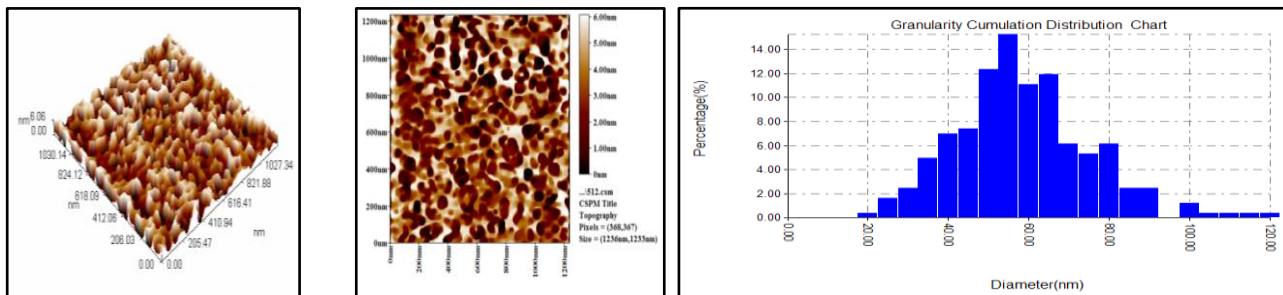
Figure (4): 2Dand 3D AFM images (upper) and size distribution of meso-porous silicon (n-type) (down) Prepared at current density 40 mA/cm² at 10 min etching time.

Table (2): The calculated morphology characteristics of n-PS for 10 min etching time

J (mA/cm²)	Roughness Average (nm)	r. m.s roughness (nm)	Average Pore Diameter (nm)	Average Pore Height (nm)
40	1.49	1.72	56.31	6.06

.
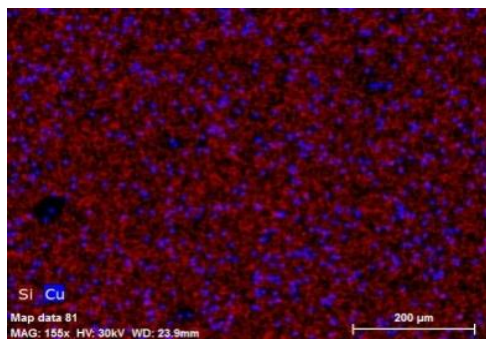
Figure (5): EXD map of elemental distribution after functionalization with Cu

3.4.   Gas Sensing Measurement

Figure (6) presents the NO₂ gas sensing properties for PS before and after functionalized with Cu which is deposited into PS substrates investigated to find the effect of Cu addition on sensitivity against NO₂ gas. Also the sensitivity is studied as a function of operating temperature to find the dependency of NO₂ gas detection on temperature. Thin films specimens are examined for gas sensing using NO₂, which is toxic gas with concentration of 25 ppm at different operation temperatures beginning from room temperature (30°C) up to 250°C with step of 50°C.

Changing in the resistivity value according to the n-type semiconductor sensor and exposure to oxidizing gas is that, in air, oxygen is adsorbed on the surface and dissociates to form

O^-, where the electron on the oxygen, is extracted from the n-type semiconductor. This electron extraction tends to increase the resistivity for the kind of n-type semiconductor where the majority charge carriers are electrons and this causes decreasing in the conductivity. Generally, when an oxidizing gas is steamed on an n-type semiconductor surface, the concentration of electrons on the surface decreases and the resistivity of the n-type semiconductor increase [9]. In general, the high values of sensitivity, which reaches more than 100% may be attributed to the optimum surface roughness, porosity, and large surface area due to porous structure.
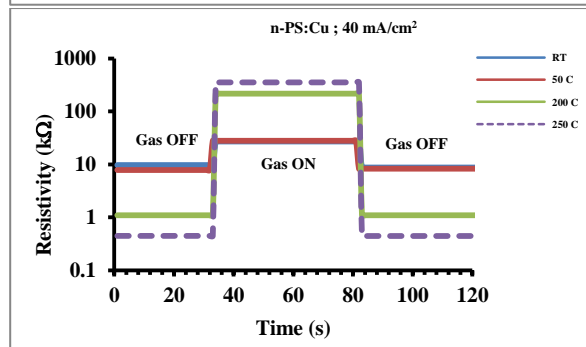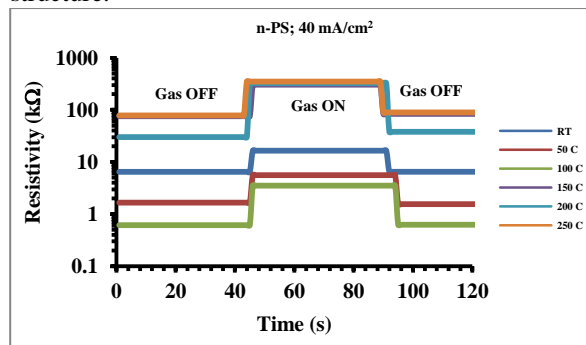
Figure (6):The variation of resistance with time for n-PS and (n-PS:Cu) with different operating temperatures for NO₂ gas sensing.

3.4.1. Operation Temperature Dependency for the sensor

Figure (7) shows the gas sensitivity tests that were performed at 30°C and increased to 250°C by 50°C step. Results show that the sensitivity at etching current 40 mA/cm^2 for NO$_2$ gas increases as the temperature increases from room temperature to 250°C as present in table (3), and it is showing a typical negative temperature coefficient of resistance (NTCR) due to the thermal excitation of the charge carriers in semiconductor. After 150°C, sensor sensitivity decreases with the increasing temperature, which led to a positive temperature coefficient of resistance (PTCR), this can attributed to the saturation of the conduction bandwidth electrons evaluate from shallow donor levels that caused by oxygen vacancies.
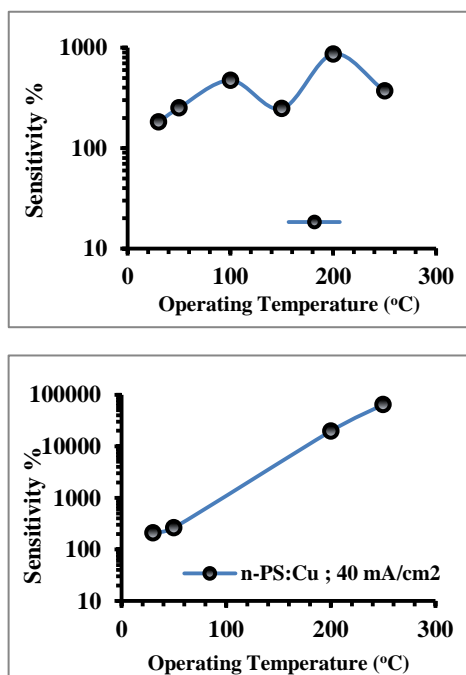
Figure (7): The variation of NO$_2$ sensitivity with the operating temperature of the PS before (upper graph) and after fictionalization with Cu (down graph).

Table (3): Sensitivity as a function of operating temperature for n-PS and (n-PS/Cu) with current density 40mA/cm^2 against NO$_2$ gas.

PS with and without metal	Sensitivity % for NO$_2$ toxic gas at operating temperatures:					
	30ºC	50ºC	100ºC	150ºC	200ºC	250ºC
n-PS	181.63	250.91	473.62	247.08	865.11	370.24
n-PS:Cu	210.530	263.62	-------	--------	19762.7	64516.8

At this point, an increase in the temperature leads to a decrease in electron mobility and a subsequent decreasing charge carriers causing high band bending due to wide depletion layer then increasing in resistance [10]. Cu atoms inside pores add charge carriers to the interface states that causes decreasing in the band bending and easy carrier transport within the junction and high temperature activates carriers to react with gas also there is large rate of oxidation[11] so the sensitivitywill increase. The maximum sensitivity to NO$_2$ gas was observed with Cu which is deposited into n-PS at 40 mA and found to be 64516.82% at the optimal temperature of 250°C.

4. CONCLUSION

Porous silicon is a promising new material for gas sensor applications with higher sensitivity more than 100 % which depended on its morphology that has a high surface-to-volume ratio due to pores formation. Fictionalization these pores with catalysts such as Cu with a very small amount improves the sensitivity of the porous structure more than 60000 % and make the device works at higher temperatures without damaging which is suitable for volcano environment or at fire cases. So the porous silicon is a material worthy of further scientific and technological investigations.

REFERENCE

1. Mohammad,J. F. "*Morphology and Electrical Properties Study of Nanocrystalline Silicon Surface Prepared By Electrochemical Etching*"**,** Iraqi Journal of Science, **57**(3A): 1707-1714(2016)
2. Canham, L. T. "*Silicon quantum wire array fabricated by electrochemical and chemical dissolution of wafers,*" Appl. Phys. Lett. , **57**(10), 159–164 (1990)
3**.** Beretta, M." *Nanostructured mesoporous materials obtained by template synthesis and controlled shape replica***,**" Ph.D.thesis. University of Milano - Bicocca Department of Materials Science,(2009).
4**.** Ozdemir, S. and Gole, J. "*The potential of porous silicon gas sensors*", Current Opinion in Solid State and Materials Science., **11**, 92-100 (2007).
5. Chen,Z., Bosman,G. and Ochoa,R. " *Visible light emission from heavily doped porous silicon homojunctionpn diodes*". Appl. Phys. Lett., **62**: 708-710(1993)
6. Khorsand, Z., Abd. Majid, W.H., Abrishami, M.E. and Ramin, Y., **"***X-ray analysis of ZnO nanoparticles by Williamson-Hall and size-strain plot methods***"**, Solid State Sciences **13**: 251-256(2011)
7**.** Omar, K., Ramizy,A. and Hassan,Z.**"***Stiffness properties of porous silicon nanowires fabricated by electrochemical and laser-induced etching***,"** Superlattices and Microstructures, **50**: 119–127 (2011)
8. Parkhutik,V. "*Porous silicon – mechanism of growth and applications,"*Solid-state Electron.,**43**: 1121-1141(1999)
9. Akamatsu, T., Itoh,T., Izu, N., and Shin,W. "*NO and NO$_2$ sensing properties of WO$_3$ and Co3O4 based gas sensors,"*Sensors (Basel)., **13**(9): 12467–12481(2013)
10. Al-Eqaby, H. "*Design and Construction of Ag, Pd and Pt dopedTiO$_2$ nanotubes as Gas Sensor,*" Ph.D. thesis. The College of Science, University of Baghdad, (2016)
11. Sxennik, E., Colak, Z., Kılınc, N. and Ziya, Z.*"Synthesis of highly-ordered TiO2 nanotubes for a hydrogen sensor,"* international journal of hydrogen energy, **35**: 4420 - 442(2010).